

COSMOLOGICAL CONSTRAINTS FROM THE REDSHIFT DEPENDENCE OF THE GALAXY ANGULAR 2-POINT CORRELATION FUNCTION

XIAO-DONG LI,

School of Physics, Korea Institute for Advanced Study, 85 Heogiro, Dongdaemun-gu, Seoul 130-722, Korea

CHENG CHENG,

Kavli Institute for Theoretical Physics China, Institute of Theoretical Physics, Chinese Academy of Sciences, Zhong Guan Cun Street 55#, Beijing, 100190, P.R. China and
 University of Chinese Academy of Sciences, P.R. China

CHANGBOM PARK,

School of Physics, Korea Institute for Advanced Study, 85 Heogiro, Dongdaemun-gu, Seoul 130-722, Korea

HYUNBAE PARK, CRISTIANO G. SABIU,

Korea Astronomy and Space Science Institute, Daejeon 305-348, Korea

JUHAN KIM¹,

Center for Advanced Computation, Korea Institute for Advanced Study, 85 Hoegi-ro, Dongdaemun-gu, Seoul 130-722, Korea and
 School of Physics, Korea Institute for Advanced Study, 85 Heogiro, Dongdaemun-gu, Seoul 130-722, Korea

AND

STEPHEN APPLEBY, SUNGWOOK E. HONG

School of Physics, Korea Institute for Advanced Study, 85 Heogiro, Dongdaemun-gu, Seoul 130-722, Korea

Draft version September 13, 2016

ABSTRACT

We use the shape of galaxy 2-point correlation function to measure the redshift dependence cosmology volume effect. ...

Keywords: large-scale structure of Universe — dark energy — cosmological parameters

1. INTRODUCTION

Dark energy ... Large scale structure...

2pCF is a good statistic... blahblah In 2d xi(s,μ)
 ... In *** we used the redshift dependence of 2pCF to probe the volume and AP effect... The method is applied to BOSS data in *** and obtain tight constraint...

In *** we further propose to use the shape of xi(s) to probe the volume effect... Stretch or compression shifts the clustering properties in some particular scale to larger or smaller scales... The shape of measured xi(s) is thus stretched or compressed.

The outline of this paper is as follows.

This paper is organized as follows... The outline of this paper proceeds as follows. In §2 we briefly review the nature and consequences of the AP effect and volume changes when performing coordinate transforms in a cosmological context. In §3 we describe the N-body simulations and mock galaxy catalogues that are used to test our methodology. In §4, we describe our new analysis method for quantifying the redshift dependence of volume effect. We conclude in §5.

2. VOLUME EFFECT IN A NUTSHELL

In this section we briefly introduce the scaling effect caused by wrongly assumed cosmological parameters. A more detailed description has been provided in Li et al. (2014, 2015, 2016).

Suppose that we are probing the size of some objects

in the Universe. We measure its redshift span Δz and angular size $\Delta\theta$, then compute its sizes in the radial and transverse directions using the following formulas

$$\Delta r_{\parallel} = \frac{c}{H(z)} \Delta z, \quad \Delta r_{\perp} = (1+z) D_A(z) \Delta\theta, \quad (1)$$

where H is the Hubble parameter and D_A is the angular diameter distance. In the particular case of a flat universe composed by a cold dark matter component and a constant EoS dark energy component, they take the forms of

$$H(z) = H_0 \sqrt{\Omega_m a^{-3} + (1 - \Omega_m) a^{-3(1+w)}}, \\ D_A(z) = \frac{1}{1+z} r(z) = \frac{1}{1+z} \int_0^z \frac{dz'}{H(z')}, \quad (2)$$

where $a = 1/(1+z)$ is the cosmic scale factor, H_0 is the present value of Hubble parameter and $r(z)$ is the comoving distance.

In case wrong values of Ω_m and w are adopted, the inferred Δr_{\parallel} and Δr_{\perp} are wrong, resulting in wrong estimation in the object's shape (AP effect) and size (volume effect). These effects and their cosmological consequences have been investigated in Li et al. (2014, 2015, 2016).

In this paper we focus on the mis-estimation of the angular size Δr_{\perp} . The ratio of mis-estimation is

$$\alpha_{\perp} \equiv \frac{\Delta r_{\perp,\text{wrong}}}{\Delta r_{\perp,\text{true}}} = \frac{D_{A,\text{wrong}}}{D_{A,\text{true}}}, \quad (3)$$

¹ Corresponding Author: kjhan@kias.re.kr

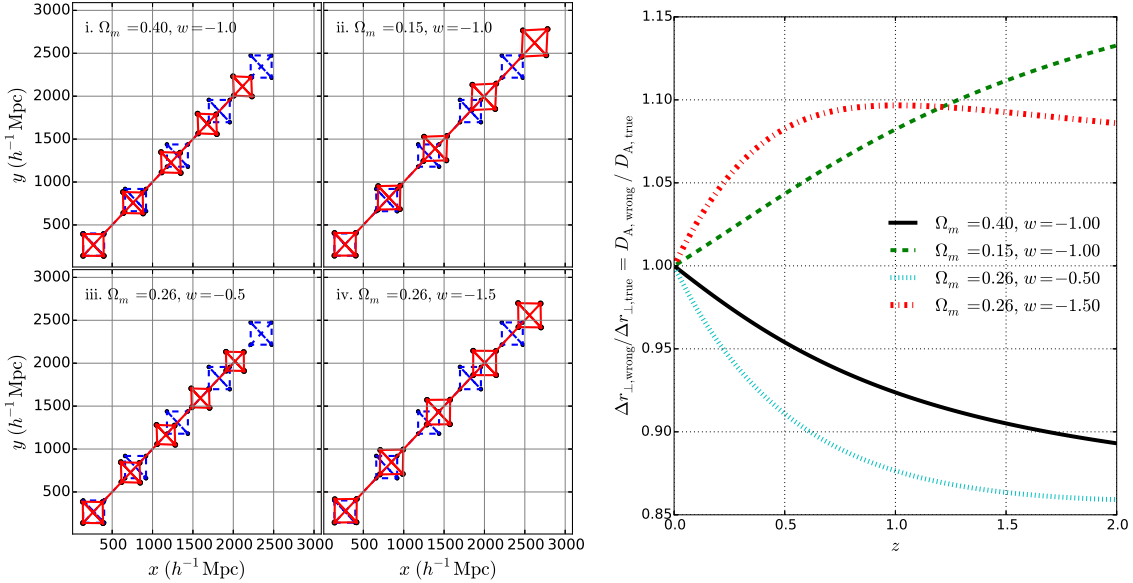


Figure 1. The scaling in four wrongly assumed cosmologies ..., assuming a true cosmology of $\Omega_m = 0.26$, $w = -1$. Left panel shows a series objects distributes as five perfect squares, measured by an observer located at the origin. Their true positions and shapes are plotted in blue dashed lines. The observer measures the redshifts of these objects, adopts the wrong cosmologies to compute the distance, and obtains wrong results (red solid lines). Right panel shows the mis-estimation of angular diameter distance when the wrong cosmologies are adopted.

where “true” and “wrong” denote the values of D_A in the true cosmology and wrongly assumed cosmologies, respectively.

An illustration is provided in the left panels of Figure 1. Suppose that the true cosmology is a flat Λ CDM with present matter ratio $\Omega_m = 0.26$ and standard dark energy EoS $w = -1$. If we were to distribute a series of perfect squares at various distances ranging from 500 Mpc/h to 3000 Mpc/h, and an observer located at the origin were to measure their redshifts and infer the sizes of the squares using the distance-redshift relations of four incorrect cosmologies

- (i). $\Omega_m = 0.40$, $w = -1.0$,
- (ii). $\Omega_m = 0.15$, $w = -1.0$,
- (iii). $\Omega_m = 0.26$, $w = -0.5$,
- (iv). $\Omega_m = 0.26$, $w = -1.5$,

as a result, the shapes of the squares appear distorted (AP effect), and their sizes are wrongly estimated (volume effect). Cosmological models (i,iii) yield to compressed size (in both angular and LOS direction), and the degree of compression increases with increasing distance;

The mis-estimation of angular size, $\Delta r_{\perp,\text{wrong}} / \Delta r_{\perp,\text{true}}$, are displayed in the right panel of Figure 1. All cosmologies, $\Delta r_{\perp,\text{wrong}} / \Delta r_{\perp,\text{true}}$ evolves a lot in the redshift range $0 < z < 2$. As an example, when adopting the quintessence cosmology $\Omega_m = 0.26$, $w = -0.5$, the angular size is underestimated by 8.9%, 12.3%, 13.6%, 14.1% at $z = 0.5, 1, 1.5, 2$.

In sum, as a consequence of incorrectly adopted cosmologies, the size of the objects is mis-estimated and the magnitude of mis-estimation depends on the redshift. In this paper we use the galaxy angular 2pCF to probe the mis-estimation of angular size $\Delta r_{\perp,\text{wrong}} / \Delta r_{\perp,\text{true}}$.

3. THE SIMULATION DATA

We test the method using the mock galaxy samples produced by the Horizon Run 4 (HR4) N-body simulation (Kim et al. 2015; Hong et al. 2016).

HR4 was made within a cube of volume $(3.15 h^{-1} \text{Gpc})^3$ using 6300^3 particles with mass $m_p \simeq 9 \times 10^9 h^{-1} \text{M}_\odot$. The simulation adopted the second order Lagrangian perturbation theory (2LPT) initial conditions at $z_i = 100$ and a WMAP5 cosmology $(\Omega_b, \Omega_m, \Omega_\Lambda, h, \sigma_8, n_s) = (0.044, 0.26, 0.74, 0.72, 0.79, 0.96)$ (Komatsu et al. 2011).

Mock galaxies are produced from the simulation based on a modified one-to-one correspondence scheme (Hong et al. 2016). The most bound member particles (MBPs) of simulated halos are adopted as tracers of galaxies. The merger timescale is computed to get the lifetime of merged halos. Merger trees of halos are constructed by tracking their MBPs from $z = 12$ to 0; when a merger event occurs, the merger timescale is computed using the formula of Jiang et al. (2008) to determine when the satellite galaxy is completely disrupted.

The resulting mock galaxies was found to reproduce the 2pCF of SDSS DR7 volume-limited galaxy sample (Zehavi et al. 2011) very well (Hong et al. 2016). The mock galaxies shows a similar finger of god (FOG) feature (Jackson 1972) as the observation. The projected 2pCF of the mock and observational samples agree within 1σ CL on scales greater than $1 h^{-1} \text{Mpc}$.

In this analysis we use snapshot data of HR4 galaxies at $z = 0, 0.5, 1, 1.5, 2$. Setting a minimal halo mass of $3 \times 10^{11} h^{-1} \text{M}_\odot$, we select 457, 406, 352, 206 and 228 million mock galaxies at the five redshifts, corresponding to a number density of 1.46, 1.30, 1.13, 0.98 and 0.73 in unit of $10^{-2} h^3 \text{Mpc}^{-3}$, respectively. By applying a uniform mass cut, at higher redshift we are selecting less galaxies with larger galaxy bias.

As an illustration, Figure 2 displays the 2D distribution of a subsample of mock galaxies in five redshifts, with x, y coordinates computed using the “correct” val-

ues of cosmological parameters $\Omega_m = 0.26$, $w = -1$ (left panels) and a wrong set of cosmological parameters $\Omega_m = 0.05$, $w = -1.5$ (right panels), respectively.

When the correct cosmology is adopted the cosmic scale is correctly estimated in five redshifts. The only factor leads to evolution of galaxy distribution with redshift is the gravitational growth of structure. With the decreasing the redshift, we clearly see how the clusters and filaments form and grow. On the other hand, when the wrong cosmology is adopted, there is an artificial scaling of scales in the constructed map. The separations among galaxies are overestimated by 25.6%, 47.3%, 62.2%, 71.7% at redshifts of 0.5, 1.0, 1.5, 2.5, leading to a clear evolution of the sizes of structures with redshift.

The growth of structure leads to growth of clustering strength of structures on all scales, while the volume effect maintain the clustering pattern and uniformly rescale all the structures. Their imprints on the large scale structure is different and should be distinguishable in the statistical analysis. In the following, we show that they affect the angular correlation function measurements in different ways, and can be easily separated.

The growth of structure also make the size of structures evolves with redshift. In the next subsection we will discuss how to distinguish these two effects in the galaxy angular 2pCF.

4. METHODOLOGY

We use the angular 2pCF as a statistical tool to probe the volume effect. The galaxy 2pCF as a function of galaxy separation in the angular direction, $\omega(r_\perp)$, is computed for snapshot data of mock galaxies at five redshifts. We adopt the Landy-Szalay estimator (Landy & Szalay 1993),

$$\omega(r_\perp) = \frac{DD - 2DR + RR}{RR}, \quad (4)$$

where DD is the number of galaxy-galaxy pairs, DR the number of galaxy-random pairs, and RR is the number of random-random pairs, all separated by a distance defined by $r_\perp \pm \Delta_{r_\perp}$ where we choose $\Delta_{r_\perp} = 1h^{-1}\text{Mpc}$. The random catalogue consists of unclustered points uniformly distributed in a same size box. In an effort to reduce the statistical variance of the estimator, we use 50 times as many random points as we have galaxies.

Considering the large number of galaxies and random points the 2pCF is computed part by part in subsamples with size of $1575 h^{-1}\text{Mpc} \times 1575 h^{-1}\text{Mpc} \times 105 h^{-1}\text{Mpc}$. The Z direction with thickness $105 h^{-1}\text{Mpc}$ is treated as the radial direction (the r direction) and the X-Y directions with each of width $1575 h^{-1}\text{Mpc}$ are the angular plane. For our simulation box size we can have 120 such subsamples. The average of the measurements in all subsamples is adopted as the 2pCF of the whole sample, while the covariances of them are adopted as the covariance matrix after multiplying a factor of $1/\sqrt{119}$.

4.1. Galaxy angular 2pCF: amplitude and shape at different redshifts

The upper-left panel of Figure 3 displays the angular 2pCF measured from HR4 mock galaxies. We multiply ω by the separation r_\perp to have similar amount of statistical uncertainty on all scales.

At different redshifts, we see large evolution in the amplitude of $\omega(r_\perp)$. The amplitude of 2pCF is proportional

to the clustering strength which is affected by the gravitational growth of structures and the bias of the galaxies. The amplitude is highest at $z = 0$ where the large scale structures experienced most gravitational growth, and also gets higher at $z > 1$ with increasing redshift as a reason of more biased galaxies at higher redshift.

Different from the large variation of amplitude among the different redshifts, the shape of $r_\perp\omega$ maintains similar at all redshifts; it always peaks at $r \sim 9h^{-1}\text{Mpc}$ and monotonically drops at larger or smaller scales. The only exception is the small enhancement at $r \lesssim 2h^{-1}\text{Mpc}$, which is caused by the non-linear growth of structures on small scales and is much more significant at lower redshift.

In order to directly compare the shape of 2pCF at different redshifts, in the middle panel of Figure 3 we show the $r_\perp\omega$ normalized by the overall amplitude within $5h^{-1}\text{Mpc} < r < 50h^{-1}\text{Mpc}$ (here after $\hat{\omega}_{r_\perp}$):

$$\hat{\omega}_{r_\perp} \equiv \frac{r_\perp\omega(r_\perp)}{\int_{r_{\perp,\min}}^{r_{\perp,\max}} r_\perp\omega(r_\perp)dr_\perp/(r_{\perp,\max} - r_{\perp,\min})}, \quad (5)$$

where we choose $r_{\perp,\min} = 5h^{-1}\text{ Mpc}$, $r_{\perp,\max} = 40h^{-1}\text{ Mpc}$ in this analysis. Scales of $r_{\perp,\min} < 5h^{-1}\text{ Mpc}$ are affected by non-linear growth of structure, the misestimation of whose contribution may lead to systematic errors in the derived cosmological constraints. On scales larger than $40h^{-1}\text{ Mpc}$ it is may be possible to have precise analytically modelling the shape of the 2pCF (Salvador et al. 2014, 2016) which should be able to extract more cosmological information than our method (although our method should is also applicable).

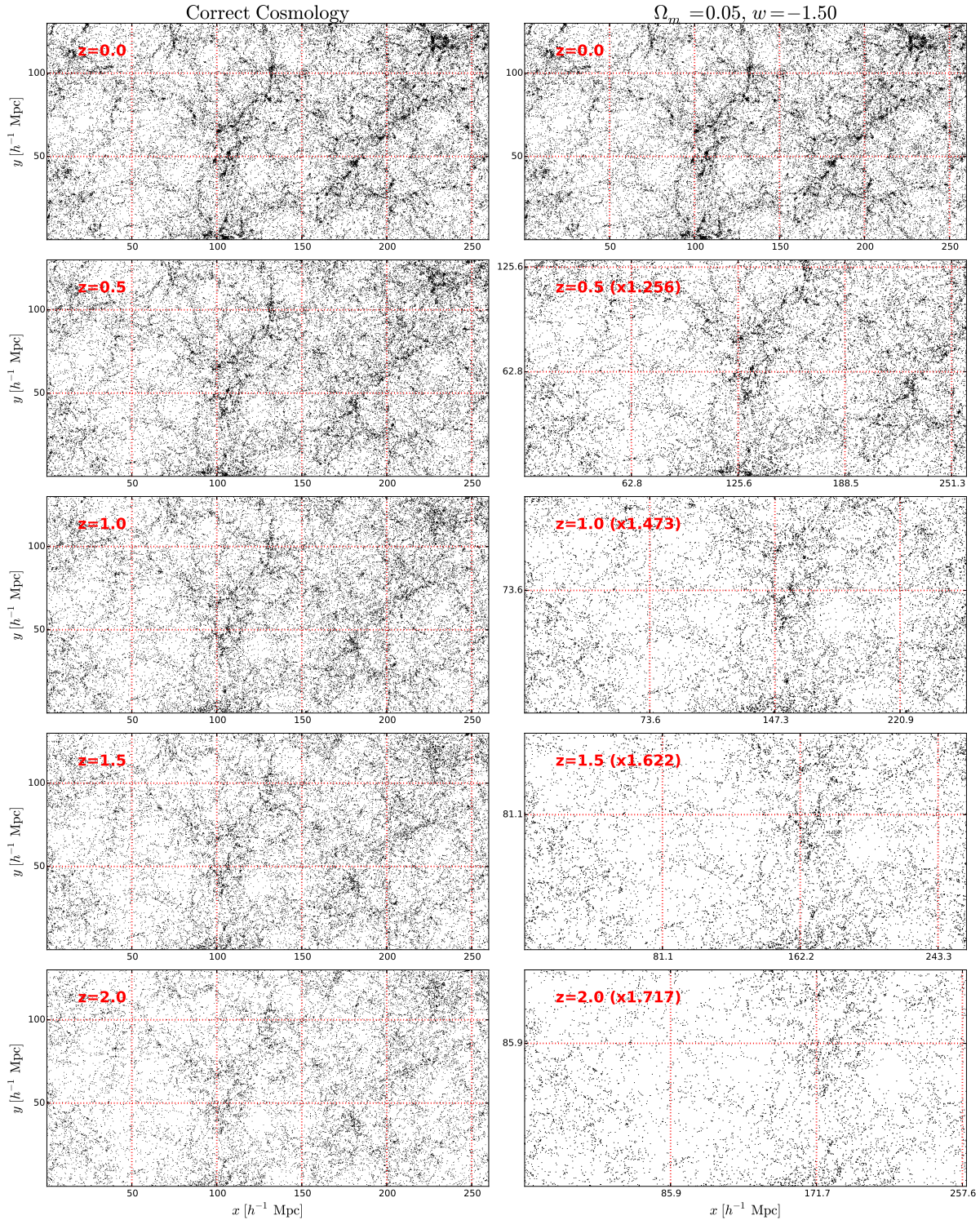
The nice overlapping of the five redshift results justify the small evolution of shape with redshift. In the right panel, we further show the residual evolution of $\hat{\omega}_{r_\perp}$ at high redshifts with respect to $z = 0$. There is only 1-4% relative enhancement at $r < 10h^{-1}\text{Mpc}$, and < 1.5% relative suppression at $r > 25h^{-1}\text{Mpc}$. The trend is monotonic with redshift.

There is one point should be emphasized here. In real observations we are observing *different* objects in different redshift shells. To mimick this we comparing slices of different redshifts at *different* locations. As an example, if at $z = 0$ we take $\hat{\omega}_{r_\perp}$ measured within $0h^{-1}\text{Mpc} < Z < 105h^{-1}\text{Mpc}$, at higher redshifts we then adopt measurement within $105h^{-1}\text{Mpc} < Z < 210h^{-1}\text{Mpc}$ for a comparision. If simply comparing the 2pCF of a *same* subsample of galaxies at different redshifts, one would significantly underestimate the statistical uncertainty of $\delta\hat{\omega}_{r_\perp}$ by ignoring the cosmic variance. The error bars and covariance are always estimated in this way to take the cosmic variance into consideration.

As shown by Figure 2, the gravitational growth of structure enhance the clustering strength of structures on all scales; here it manifests itself as an enhanced amplitude of 2pCF at low redshift. The shape of 2pCF, which represents the *relative strength of clustering among different scales*, maintain similar with redshift except the non-linear scales of $r_\perp < 5h^{-1}\text{Mpc}$.

4.2. Galaxy angular 2pCF: Cosmological Effect

The measured angular correlation function of galaxies with positions constructed using the wrong cosmology $\Omega_m = 0.05$, $w = -1.5$ is displayed in the lower panels of Figure 3. The mis-scaling uniformly shifts clustering

**Figure 2.** blah

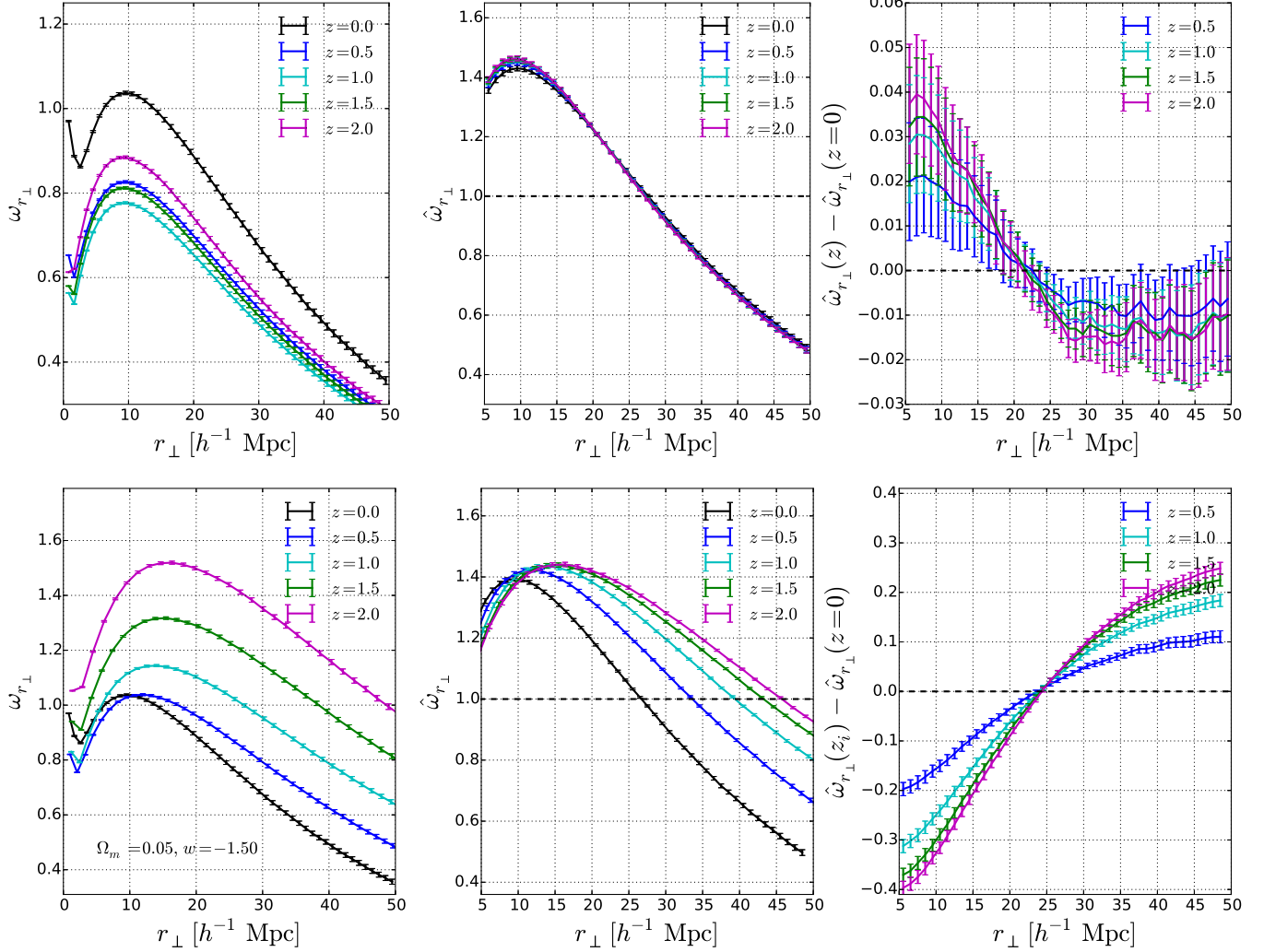


Figure 3. 2pCF at different redshifts.

patterns on all scales, lead to a wrong estimation of $\hat{\omega}_{r\perp}$ related with the correct one as

$$\hat{\omega}_{r\perp,\text{wrong}}(r) = \hat{\omega}_{r\perp,\text{correct}}(\alpha_{\perp} r), \quad (6)$$

a simple consequence of the phenomenon that clustering patterns at distance r now appears on $\alpha_{\perp} r$. The redshift evolution of α_{\perp} leads to redshift evolution of shape.

The change in shape as well as the redshift evolution is displayed in the middle panel. The upscaling of comoving distance lead to a stretched shape. With the increasing of redshift, the peak location is shifted from $9h^{-1}\text{Mpc}$ to $15h^{-1}\text{Mpc}$ at $z = 2$, as a result of the fact that the angular separation is upscaled by 71.7%. Correspondingly, the right panel shows that, compared with $\hat{\omega}_{r\perp}$ at $z = 0$ there is a 20-40% change at higher redshifts.

The mis-scaling not only changes the of the 2pCF but also modifies its amplitude. as shown in the left panel, due to the stretch of scale the amplitude is enhanced at higher redshifts; the higher the redshift, the more the enhancement.

Although the change of amplitude could be a more significant consequence of wrong cosmology than the alteration of shape, it is mixed with other factors; the growth of structure and a larger galaxy bias can also lead to a stronger clustering and thus an enhanced amplitude of 2pCF. In the analysis to extract cosmological information, we just make use of the redshift evolution of the 2pCF shape, which is less affected by factors of structure growth and galaxy bias.

4.3. Systematic effects

Sec. 4.1 shows that $\hat{\omega}_{r\perp}$ measured from a set of constant mass cut samples at different redshifts is close to each other. The gravitational growth of structure will not have a large impact on $\hat{\omega}_{r\perp}$ on scales $\gtrsim 5h^{-1}\text{Mpc}$. The other factors may introduce redshift evolution of the clustering of measured galaxies include the redshift space distortion (RSD), galaxy bias, redshift error, and other properties of galaxies, such as the mass, morphology, color, concentration. Here we test two “major” systematical effects, the galaxy bias and the RSD effect.

4.3.1. Galaxy Bias

Galaxies are biased tracers of dark matter field; more massive galaxies reside in regions with higher density contrast. In large scale structure surveys, the bias of the galaxy sample is an important fator affecting on the clustering properties of the sample.

We check the effect of galaxy bias on $\hat{\omega}_{r\perp}$. The upper panels of Figure 4 displays the 2pCF measured from galaxies within a $3175 \times 3175 \times 105$ ($h^{-1}\text{Mpc}$)³ volume, taken from the $z = 0$ snapshot. Four values of minimal mass limits, $3 \times 10^{11} M_{\odot}$, $1 \times 10^{12} M_{\odot}$, $4 \times 10^{12} M_{\odot}$ and $1 \times 10^{13} M_{\odot}$, are imposed to create three samples with different galaxy bias. The measured angular 2pCF are displayed.

The different mass cuts result in large variation in the amplitude of the 2pCF (left panel), while the shape of the 2pCF remains less affected (middle panel). Compared with the sample of $M > 3 \times 10^{11} M_{\odot}$, samples with mass limits of $1 \times 10^{12} M_{\odot}$, $4 \times 10^{12} M_{\odot}$ and $1 \times 10^{13} M_{\odot}$ have amplitude of 2pCFs enhanced by 10%, 50% and 100%, while the change in $\hat{\omega}_{r\perp}$ is only 0.5%, 2% and 4%. So the effect of galaxy bias is much avoided by utilizing the shape of the 2pCF rather than the amplitude.

4.3.2. Redshift Space Distortion

The galaxy peculiar velocity contributes to the observed redshift and distorted the inferred galaxy radial position, known as the redshift space distortion. It is the major systematics in our previous works (Li et al. 2014, 2015, 2016) where we derive cosmological constraints from the redshift evolution of the 3D galaxy distribution.

The effect of RSD is expected to be much milder in this work. The angular positions of the galaxies is not shifted by RSD at all; the only effect of RSD come in the procedure of sample preparation. The galaxies observed in a survey are split into shells of subsamples with different redshift ranges for the purpose 2pCF measurement. RSD disortes the galaxy redshift and as a result some galaxies (especially those close to the boundaries of shells) could be classified to wrong redshift shells.

The lower panel of Figure 4 displays the RSD effect on 2pCF. To have the effect of RSD we shift the radial coordinates of galaxies according to the relation

$$\Delta z = (1 + z) \frac{v_z}{c}, \quad (7)$$

where v_{LOS} is the galaxy peculiar velocity in the radial direction. This lead to mis-classification of some galaxies when we split the box into slices.

Comparing the plot with Figure 3 one clearly see the effect of RSD. The amplitude of measured 2pCF is enhanced by $\sim 10\%$ in case of considering the RSD effect. The slop of $\hat{\omega}_{r\perp}$ slightly suppressed. While the redshift evolution of $\hat{\omega}_{r\perp}$ is still small... Although the pattern is a little modified... So RSD is not a big issue here... **after anna jobs finished we have better plots and re-revise this section**

Similar to RSD, redshift errors of galaxies (typically 0.02 for photometric survey) also results in fuzzy boundaries of shells and mis-classification of galaxies. This effect should also be properly quantified in real observations.

4.4. Likelihood Analysis

We design the likelihood function to quantify the redshift evolution of $\hat{\omega}_{r\perp}$. A cosmology resulting in smaller evolution is considered to be more likely the correct one. The procedure here is very similar to what we did in Li et al. (2014, 2015, 2016). We compare the high redshift $\hat{\omega}_{r\perp,\text{perp}}$ and the lowest redshift measurement:

$$\chi^2 \equiv \sum_{i=2}^{n_z} \sum_{j_1=1}^{n_r} \sum_{j_2=1}^{n_r} \mathbf{p}(z_i, r_{j_1}) (\mathbf{Cov}_i^{-1})_{j_1, j_2} \mathbf{p}(z_i, r_{j_2}), \quad (8)$$

where n_z is the number of redshifts which is 5 in this analysis, n_r is number of binning in $\hat{\omega}_{r\perp}(r_{\perp})$, which is 35 since we have r_{\perp} bins with width $1h^{-1}\text{Mpc}$ in a range of $5h^{-1}\text{Mpc} \leq r \leq 40h^{-1}\text{Mpc}$. $\mathbf{p}(z_i, r_j)$ is the redshift evolution of the angular correlation function shape with systematic effects subtracted

$$\mathbf{p}(z_i, r_j) \equiv \delta r_{\perp} \omega(z_i, z_1, r_j) - \delta r_{\perp} \hat{\omega}_{\text{sys}}(z_i, z_1, r_j) \quad (9)$$

\mathbf{Cov}_i is the covariance matrix estimated from the $\mathbf{p}(z_i, r_j)$ measured from 120 subsamples. As mentioned before, for a robust estimation of covariance matrix, we always compare slices at different locations to include the cosmic variance.

The covariance matrix inferred from a finite number of samples is always a biased estimate of the true matrix

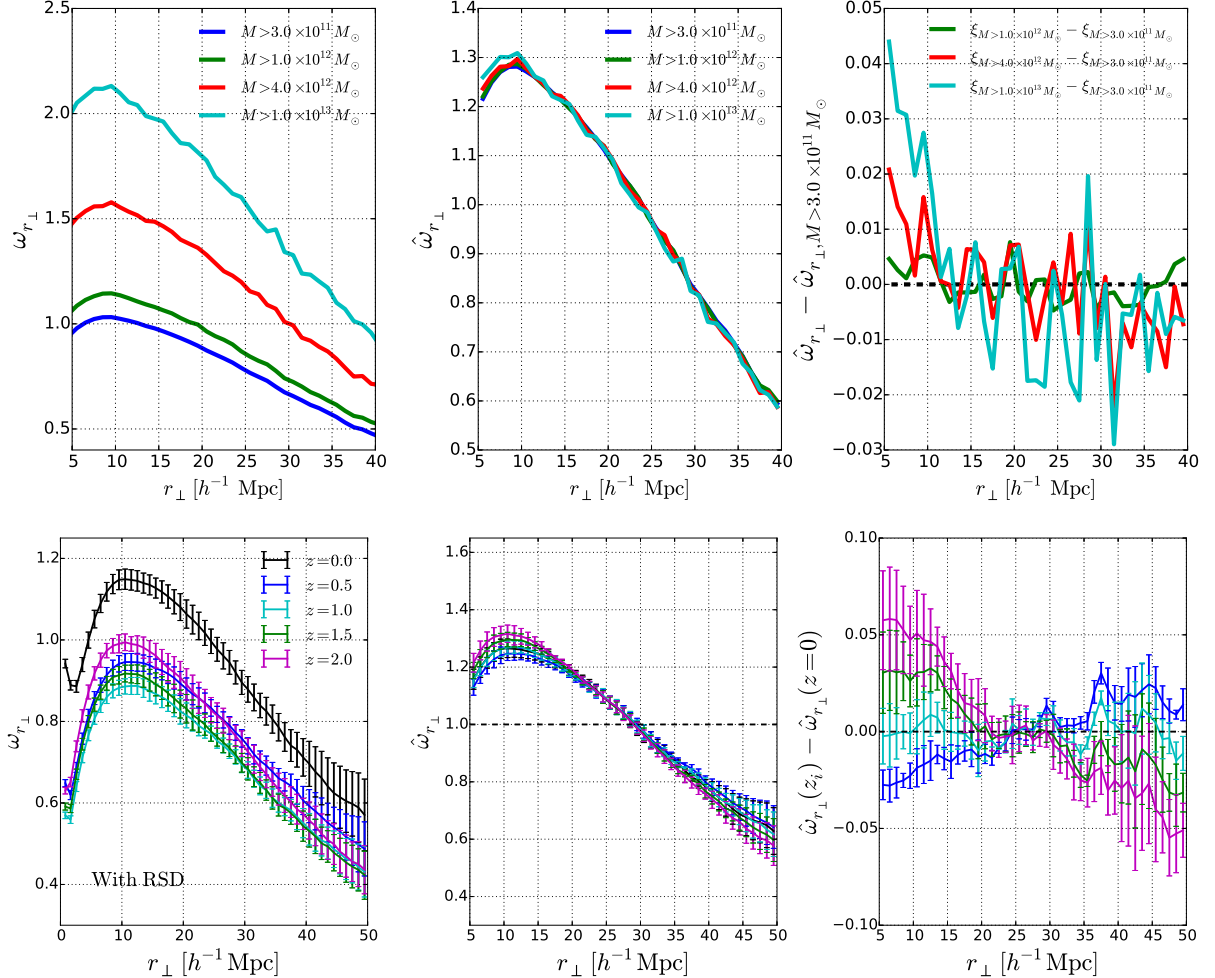


Figure 4. Systematic effects.

(Hartlap et al. 2006). This can be corrected by rescaling the inverse covariance matrix as

$$\mathbf{Cov}_{ij, \text{Hartlap}}^{-1} = \frac{N_s - n_r - 2}{N_s - 1} \mathbf{Cov}_{ij}^{-1}, \quad (10)$$

where \$N_s = 120\$ is the number of mocks used in covariance estimation. For the options of this analysis the rescaling is as large as 1.43. In the case that one have 2 000 mocks the rescaling is less than 1.02.

Figure 5 displays the 2pCF and the likelihood values in case of adopting the four wrong cosmologies of Figure 1. For the cosmologies \$\Omega_m = 0.4, w = -1\$ and \$\Omega_m = 0.26, w = -0.5\$, the compression of structure shift the large scale clustering patterns into small scales, and also becomes more significant at higher redshift. We get 2pCFs with steeper slope and the higher the redshift the steeper. For cosmologies \$\Omega_m = 0.15, w = -1\$ and \$\Omega_m = 0.26, w = -1.5\$, the stretch of structure leads to shallower slope of \$\hat{\omega}_{r\perp}\$ and the higher the redshift the shallower. In all cosmologies we have significant detection of redshift evolution. We computed the \$\chi^2\$ values according to Equation 8, and found these cosmological parameters are strongly disfavored at \$\gtrsim 30\sigma\$ CL.

5. COSMOLOGICAL CONSTRAINT

We constrain \$\Omega_m\$ and \$w\$ through Bayesian analysis (Christensen et al. (2001); also see Lewis & Bridle

(2002); Li et al. (2016)). We assume the likelihood takes the form

$$\mathcal{L} \propto \exp \left[-\frac{\chi^2}{2} \right] \quad (11)$$

and scan the parameter space in \$\Omega_m - w\$ plane to obtain the 68.3% and 97.4% CL regions. The result is displayed in Figure 6.

We get tight constraint on the two parameters. The \$2\sigma\$ contour lies within the region \$0.23 < \Omega_m < 0.285\$, \$-1.1 < w < -0.9\$. The thin shape of contour means, when combining with the another observational data with different direction of degeneracy (e.g. CMB), very tight combined constraint can be obtained. In case of fixing one parameter at its best-fit value and infer the statistical uncertainty of the other one, one will obtain \$1\sigma\$ uncertainty of \$\delta\Omega_m \approx 0.002, \delta w \approx 0.01\$.

6. CONCLUDING REMARKS

* Can be combined with our redshift dependence of AP to full explore the geometric effects in LSS

* *** utilizes angular 2pCF as a function of redshift. Our method is complementary to it: 1) smaller scales; 2) more bins; 3) could be less affected by RSD; ... In case of good modelling of RSD one can rely on their; in case not possible, especially on small scales, one can use ours

* Complementary to all other LSS probes

* Promising future

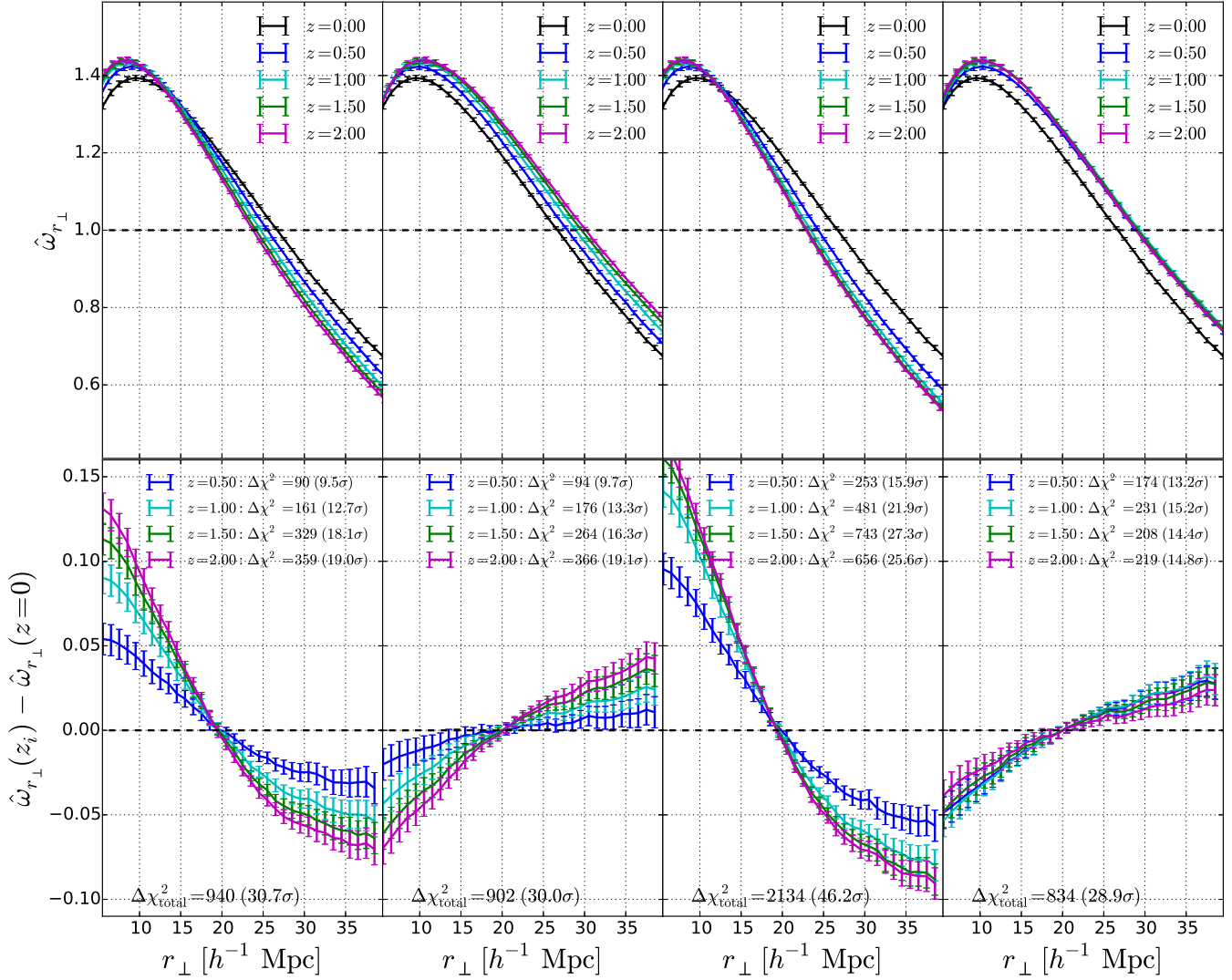


Figure 5. 2pCF in cosmologies.

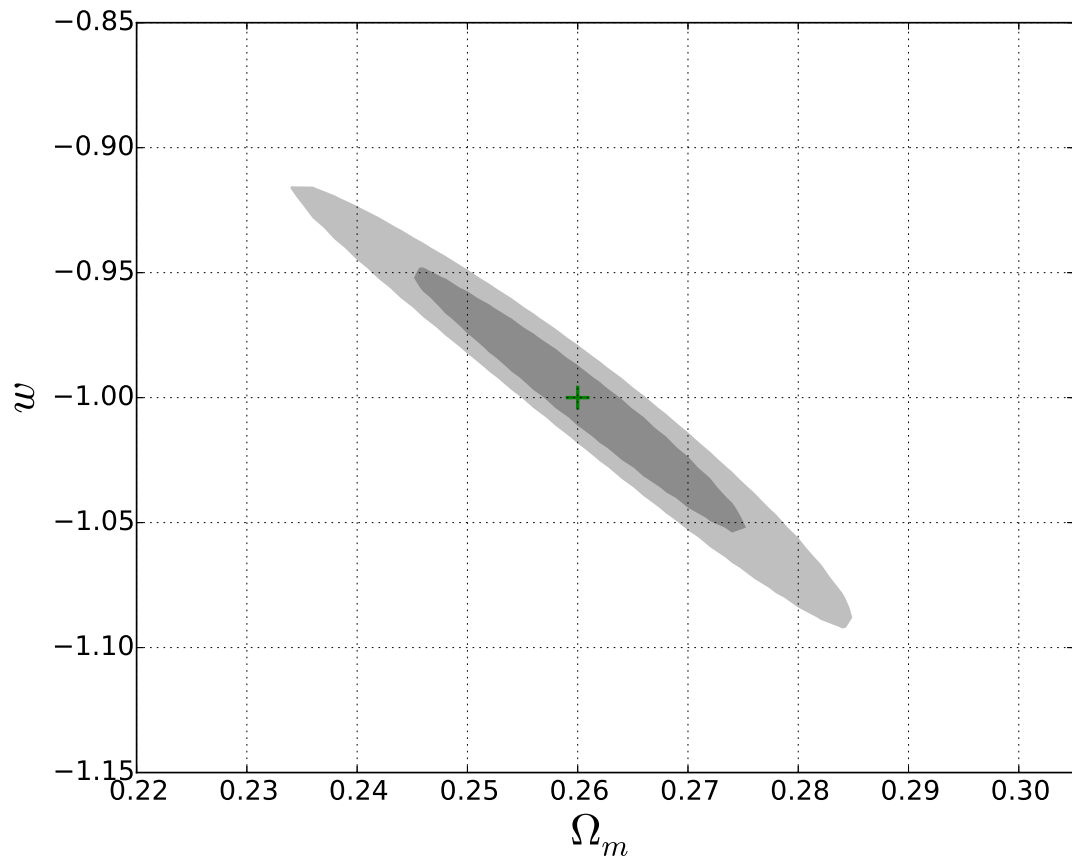


Figure 6. Likelihood contours (68.3%, 95.4%) in the $\Omega_m - w$ plane from our method.

ACKNOWLEDGMENTS

We thank the Korea Institute for Advanced Study for providing computing resources (KIAS Center for Advanced Computation Linux Cluster System). We would

like to thank Yi Zheng for useful discussions. This work was partially supported by the Supercomputing Center/Korea Institute of Science and Technology Information with supercomputing resources including technical support (KSC-2013-G2-003).

APPENDIX

REFERENCES

- Ade, P.A.R., Aghanim, N., & Arnaud, M., et al. arXiv:1502.01589
- Alam, S., Ata, M., & Bailey, S., et al. 2016, submitted to MNRAS (arXiv:1607.03155)
- Alam S., Albareti, F.D., & Allende Prieto, C., et al., 2015, ApJS, 219, 12
- Alcock, C., & Paczynski, B. 1979, Nature, 281, 358
- Anderson, L., Aubourg, É., & Bailey, S. et al. 2014, MNRAS, 441, 24
- Ballinger, W.E., Peacock, J.A., & Heavens, A.F. 1996, MNRAS, 282, 877
- Betoule, M., Kessler, R., & Guy, J., et al. 2014, A&A, 568, 32
- Beutler, F., Blake, C., & Colless, M., et al. 2011, MNRAS, 416, 3017
- Beutler, F., Saito, S., & Seo, H.-J., et al. 2013, MNRAS, 443, 1065
- Beutler, F., Seo, H.-J., & Saito, S., et al. 2016, arXiv:1607.03150
- Blake, C., Glazebrook, K., & Davis, T. M., 2011, MNRAS, 418, 1725
- Blake, C., James, J.B., & Poole, G.B. 2013, MNRAS, 437, 2488
- Bolton, A.S., Schlegel, & D.J., Aubourg E., et al. 2012, AJ, 144, 144
- Boylan-Kolchin, M., Ma, C.-P., & Quataert, E. 2008, MNRAS, 383, 93
- Christensen, N., Meyer, R., Knox, L., & Luey, B. 2001, Class. Quant. Grav., 18, 2677
- Chuang, C.-H., & Wang, Y. 2012, MNRAS, 426, 226
- Dawson, K.S., Kneib, J.P., & Percival, W.J., et al. 2015, accepted AJ
- Dawson, K.S., Schlegel, D.J., & Ahn, C.P., et al. 2012, AJ, 145, 10
- Efstathiou, G. 2014, MNRAS, 440, 1138
- Eisenstein, D.J., Weinberg, D.H., & Agolet, E., et al. 2011, AJ, 142, 72
- Feldman, H.A., Kaiser, N., & Peacock, J.A. 1994, ApJ, 426, 23
- Fukugita, M., Ichikawa, T., & Gunn, J.E., et al. 1996, AJ, 111, 1748
- Gunn, J.E., Carr, M., & Rockosi, C. et al. 1998, AJ, 116, 3040
- Gunn, J.E., Siegmund, W.A., & Mannery, E.J., et al. 2006, AJ, 131, 2332
- Guzzo, L., Pierleoni, M., & Meneux, B., et al. 2008, Nature, 451, 541
- Hartlap J., Simon P. & Schneider P. [astro-ph/0608064].
- Hong, S.E., Park, C., & Kim, J. 2016, ApJ, 823, 103
- Jackson, J. 1972, MNRAS, 156, 1
- Jennings, E., Baugh, C.M., & Pascoli, S. 2011, MNRAS, 420, 1079
- Jiang, C.Y., Jing, Y. P., & Faltenbacher, A., et al. 2008, ApJ, 675, 1095
- Kaiser, N. 1987, MNRAS, 227, 1
- Kim, J., & Park, C. 2006, ApJ, 639, 600
- Kim, J., Park, C., Gott, J.R., III, & Dubinski, J. 2009, ApJ, 701, 1547
- Kim, J., Park, C., L'Huillier, B., & Hong, S. E. 2015, JKAS, 48, 213
- Kim, J., Park, C., Rossi, G., Lee, S.M., & Gott, J.R. 2011, JKAS, 44, 217
- Kitaura, F.S., Rodríguez-Torres, S., Chuang, C.-H., et al. arXiv:1509.06400
- Komatsu, E., Smith, K. M., & Dunkley, J., et al. 2011, ApJS, 192, 18
- Lacey, C., & Cole, S. 1993, MNRAS, 262, 627
- Landy, S.D., & Szalay, A.S. 1993, ApJ, 412, 64
- Laureijs, R., Amiaux, J., & Arduini, S., et al. 2011, arXiv:1110.3193
- Lavaux, G., & Wandelt, B.D. 2012, ApJ, 754, 109
- Lewis, A., & Bridle, S. 2002, Phys. Rev. D, 66, 103511
- L'Huillier, B., Park, C., & Kim, J. 2014, New Astronomy, 30, 79
- Li, M., Li, X.-D., Wang, S., & Wang, Y. 2011, Commun. Theor. Phys., 56, 525
- Li, X.-D., Park, C., Forero-Romero, J., & Kim, J. 2014, ApJ, 796, 137
- Li, X.-D., Park, C., Sabiu, C.G., & Kim, J. 2015, MNRAS, 450, 807
- Li, X.-D., Park, C., Sabiu, C.G., & Kim, J. 2016, submitted to ApJ
- Linder, E.V., Minji, O., Okumura, T., Sabiu, C.G., & Song, Y.-S. 2014, Phys. Rev. D, 89, 063525
- López-Corredoira, M. 2014, ApJ, 781, 96
- Marinoni, C., & Buzzi, A. 2010, Nature, 468, 539
- Matsubara T., & Suto, Y. 1996, ApJ, 470, L1
- McCavana, T., Micic, M., Lewis, G. F., et al. 2012, MNRAS, 424, 361
- Morandi, A., & Sun, M. arXiv:1601.03741
- Outram, P.J., Shanks, T., Boyle, B.J., Croom, S.M., Hoyle, F., Loaring, N.S., Miller, L., & Smith, R.J. 2004, MNRAS, 348, 745
- Parejko J.K., et al., 2013, MNRAS, 429, 98
- Parihar, P., Vogeley, M.S., & Gott, J.R., et al. 2014, ApJ, 796, 86
- Park, C., Kim, J., & Gott, J.R. 2005, ApJ, 633, 1
- Park, C., & Kim, Y.-R. 2010, ApJL, 715, L185
- Park, C., Choi, Y.-Y., Kim, J., Gott, J.R., Kim, S.S., & Kim, K.-S. 2012, ApJ, 759, 7
- Park, C., Song, H., Einasto, M., Lietzen, H., & Heinamaki, P. 2015, JKAS, 48, 75
- Peebles, P.J.E., & Ratra, B. 2003, Reviews of Modern Physics, 75, 559
- Percival, W.J., Ross, A.J., & Sánchez, A.G., et al. 2014, MNRAS, 439, 2531
- Perlmutter, S., Aldering, G., & Goldhaber, G., et al. 1999, ApJ, 517, 565
- Press, W.H., & Schechter, P.L. 1974, ApJ, 187, 425
- Reid, B., Samushia, L., & White, M., et al. 2012, MNRAS, 426, 2719
- Reid, B., Ho, S., & Padmanabhan, N., et al. 2016, MNRAS, 455, 1553
- Riess, A.G., Filippenko, A.V., & Challis, P., et al. 1998, AJ, 116, 1009
- Riess, A.G., Macri, L., & Casertano, S., et al. 2011, ApJ, 730, 119
- Ross, A.J., Percival, W.J., & Sánchez, A.G. et al. 2012, MNRAS, 424, 564
- Ross, A.J., Samushia, L., & Howlett, C., et al. 2015, MNRAS, 449, 835
- Ryden, B.S. 1995, ApJ, 452, 25
- Salvador, S.A., Sánchez, A.G., Padilla, N.D., & Baugh, C.M. 2014, MNRAS, 443, 2612
- Salvador, S.A., Sánchez, A.G., & Grieb, J.N., et al. 2016, submitted to MNRAS
- Sanchez, A. G., Scoccimarro, R., & Crocce, M., et al. arXiv:1607.03147
- Schlaflay E.F., Finkbeiner D.P., Schlegel D.J., et al. 2010, ApJ, 725, 1175
- Schlaflay E.F., & Finkbeiner D.P. 2011, ApJ, 737, 103
- Schlegel, D., Abdalla, F., & Abraham, T., et al. 2011, arXiv:1106.1706
- Smee, S.A., Gunn, J.E., & Uomoto, A., et al. 2013, AJ, 146, 32
- Song, Y.S., Sabiu, C.G., Okumura, T., Oh, M., & Linder, E.V. 2014, JCAP, 12, 005
- Speare, R., Gott, J.R., Kim, J., & Park, C. 2015, ApJ, 799, 176
- Viana, P.T.P., & Liddle, A.R. 1996, MNRAS, 281, 323
- Villalobos, Á., De Lucia, G., Weinmann, S.M., Borgani, S., & Murante, G. 2013, MNRAS, 433, L49
- Weinberg, S. 1989, Reviews of Modern Physics, 61, 1
- White M., et al. 2011, ApJ, 728, 126

- York, D.G., Adelman, J., & Anderson, J.E., et al. 2000, AJ, 120, 1579 Zehavi, I., Zheng, Z., & Weinberg, D.H., et al. 2011, ApJ, 736, 59